Research Square

Preprints are preliminary reports that have not undergone peer review.
They should not be considered conclusive, used to inform clinical practice,
or referenced by the media as validated information.

Integrated phosphorus management strategy improves maize phosphorus use efficiency by coordinating root-zone phosphorus availability and root architecture under reduced-P drip irrigation

Yuxiang Li

yxli@shzu.edu.cn

Shihezi University https://orcid.org/0009-0008-8025-3185

Qingyun Tang
Guojiang Yang
Zhong Zheng
Jiahui Hao
Xin Zhu
Kexing Xie
Zhijian Gao
Yali Zhang
Guodong Wang

Research Article

Keywords: Drip-irrigated maize, banded deep P placement, Hedley P fractionation, root architecture, phosphorus use efficiency, root-soil coupling

Posted Date: July 23rd, 2026

DOI: https://doi.org/10.21203/rs.3.rs-10066941/v1

License: This work is licensed under a Creative Commons Attribution 4.0 International License.
Read Full License

Integrated phosphorus management strategy improves maize phosphorus use efficiency by coordinating root-zone phosphorus availability and root architecture under reduced-P drip irrigation

Qingyun Tang [a*], Guojiang Yang [b*], Zhong Zheng [a], Jiahui Hao [a], Xin Zhu [a], Kexing Xie [a], Zhijian Gao[b], Yali Zhang [a✉], Guodong Wang [b✉], Yuxiang Li [a✉]

[a] *Key Laboratory of Oasis Ecological Agriculture of Shihezi University/Xinjiang Production and Construction Corps, Shihezi, 832003, China*

[b] *Northwest Oasis Water-saving Agriculture Key Laboratory, Ministry of Agriculture and Rural Affairs/Xinjiang Production & Construction Corps Key Laboratory of Efficient Utilization of Water and Fertilizer, Shihezi, Xinjiang, 832000, China*

Abstract:

Background and aims In calcareous soils, Ca^{2+}-mediated P fixation and surface P accumulation limit the spatial matching between P supply and roots, reducing maize P uptake and PUE. This study evaluated whether integrated P management combining banded deep P placement with γ-polyglutamic acid (γ-PGA) could sustain maize yield and improve PUE under reduced P input.

Methods A two-year field experiment was conducted in 2024-2025 with two maize cultivars and five P treatments: no P (P0), conventional P (P1), 20% reduced P (P2), 20%

* Indicates the authors who contributed equally to this study

✉ Corresponding author at: Key Laboratory of Oasis Ecological Agriculture of Shihezi University/Xinjiang Production and Construction Corps, Shihezi, 832003, China. Northwest Oasis Water-saving Agriculture Key Laboratory, Ministry of Agriculture and Rural Affairs/Xinjiang Production & Construction Corps Key Laboratory of Efficient Utilization of Water and Fertilizer, Shihezi, Xinjiang, 832000, China.
E-mail address: zhangyali_cn@foxmail.com (Y. Zhang); 95201209@163.com (G. Wang); yxli@shzu.edu.cn (Y. Li).

reduced P plus γ-PGA (P3), and 20% reduced P plus γ-PGA with deep P placement (P4). *Results* Compared with P1, P2 reduced yield by 7.6%-21.5% and significantly decreased plant P accumulation and PUE. P3 maintained yield and partly alleviated reductions in P accumulation and root growth. P4 maintained yield, increased PUE by 15.6%-27.1%, reduced apparent P balance by 51.3%-64.8%, and increased the Post-anthesis P contribution to grain by 8.5%-15.2%. P4 increased root length, root volume, and crossings, promoted very fine root proliferation and deeper root distribution, and improved root fractal characteristics. In the 30-40 cm soil layer, Resin-P, $NaHCO_3$-Po, and available P increased by 26.8%, 20.8%, and 31.2%-38.5%, respectively. PLS-PM indicated that active P fractions were closely associated with root architectural optimization and plant P accumulation. *Conclusion* Integrated P management effectively reconstructed root-soil spatial coupling, enabling high yield and efficient P utilization under reduced P input in drip-irrigated calcareous soils.

Keywords: Drip-irrigated maize; banded deep P placement; Hedley P fractionation; root architecture; phosphorus use efficiency; root-soil coupling

Introduction

Phosphorus (P) is an essential macronutrient governing cellular energy metabolism, nucleic acid synthesis, and crop yield formation (Jiang et al. 2021; Yang et al. 2021a). However, global phosphate rock reserves are finite and non-renewable, with peak consumption projected within this century (McDowell et al. 2024). Paradoxically, over 73% of global croplands exhibit suboptimal available P, creating a dual challenge of

resource scarcity and inefficient utilization (Withers 2019; Gong et al. 2025a). Long-term excessive P application has resulted in substantial legacy P accumulation in soils, yet much of this P remains biologically unavailable due to strong soil fixation processes (Guo et al. 2024). This not only reduces resource-use efficiency but also exacerbates eutrophication risks through runoff and leaching losses (McDowell et al. 2024; Guo et al. 2025). Therefore, developing strategies to improve P-use efficiency while reducing fertilizer inputs and mobilizing legacy soil P has become a critical imperative for sustainable agriculture development.

In the arid and semi-arid regions of northwestern China, plastic-mulch drip-irrigated maize underrepresents the dominant cropping systems. However, the widely distributed calcareous soils (pH >8.0) in this region impose unique and severe constraints on P cycling. Phosphate ions ($H_2PO_4^-$/HPO_4^{2-}) readily react with abundant Ca^{2+} to form sparingly soluble calcium phosphate minerals (Shen et al. 2011; Zhou et al. 2026). Consequently, P diffusion in soil is extremely limited (approximately 0.13 mm d^{-1}), far slower than root elongation rates (Lombi et al. 2005), making P availability highly dependent on fertilizer placement rather than total application rates. Phosphorus availability is determined not only by total soil P, but also by the coupled effects of its chemical forms and spatial distribution(Yang et al. 2021a). According to the Hedley P fractionation framework, soil P can be divided into a labile pool directly available to plants (Resin-P and $NaHCO_3$-Pi), a moderately labile pool with slower release rates (NaOH-Pi), and a stable pool dominated by sparingly soluble Ca-bound P (HCl-P) (Hedley et al. 1982).

Previous studies have demonstrated that deep fertilizer placement can relocate nutrients into the active rooting zone, thereby promoting deep root growth and improving nutrient acquisition efficiency (Alam et al. 2018; Ma et al. 2021; Chen et al. 2024a). Deep placement creates localized high-P environment within a limited soil volume, increasing P concentration in the soil solution at the fertilizer placement site, reducing fertilizer-soil contact, alleviating P fixation, and strengthening localized P supply intensity (Vandamme et al. 2018). However, deep placement alone cannot effectively activate legacy P pools or address the fundamental issue of Ca^{2+}-mediated P fixation in calcareous soils. Concurrently, phosphorus efficiency enhancers also represent another promising strategy. Among these, γ-polyglutamic acid (γ-PGA) can activate the release of slowly available, and moderately active soil phosphorus (NaOH-Pi) and stable phosphorus primarily bound to calcium HCl-P (Zeng et al. 2024), thereby increasing phosphorus uptake and utilization efficiency by crops (Liang and Shi 2021), promoting crop growth and yield improvement (Wang et al. 2025), and enhancing crop adaptability to abiotic stresses. Nevertheless, γ-PGA applied alone cannot resolve the spatial mismatch between P supply zones and root distribution in deep soil layers. Therefore, integrating γ-PGA with banded deep phosphorus placement may provide complementary functions by simultaneously improving phosphorus activation and optimizing the spatial positioning of phosphorus supply. However, whether such an integrated strategy enhances root-soil spatial coupling under reduced phosphorus input remains largely unknown.

Roots constitute the primary interface for soil nutrient acquisition, and root

morphology and architecture exert strong control over P uptake (Postma and Lynch 2011; Sun et al. 2022). In recent years, root architecture has emerged as a critical framework for understanding plant adaptation to spatially heterogeneous nutrient environments. Root branching patterns, topological traits, and fractal characteristics can quantitatively describe the spatial exploration capacity of roots and their resource acquisition efficiency (Lynch 1995; York et al. 2016; Wang et al. 2020a). Fitter (1986, 1987) proposed that root topology reflects branching patterns in soil, with dichotomous and herringbone branching representing two extreme architectural types (Fitter 1986; Fitter et al. 1991). Fractal dimension and fractal abundance characterize the space-filling capacity and competitive ability of roots, providing an integrated reflection of plant nutrient acquisition strategies (Wang et al. 2009; Beidler et al. 2015; Chun et al. 2021; Loudari et al. 2022). Although previous studies have shown that deep placement or water-fertilizer regulation can affect root length and root surface area, systematic quantitative evidence is still lacking regarding how integrated P management strategies optimize root architecture to improve nutrient acquisition and how these responses are coupled with changes in soil P fractions.

Although previous studies have shown that deep placement can improve nutrient delivery to the active rooting zone and that γ-PGA can enhance nutrient retention and P activation in the rhizosphere, these studies have largely focused on their individual effects. It remains unclear whether, under reduced-P input in calcareous drip-irrigated systems, the combined strategy can simultaneously promote the downward redistribution of active P fractions, induce root architectural optimization in subsoil

layers, and ultimately enhance the coordination between soil P supply and plant P uptake. Quantitative evidence is still lacking on whether changes in soil P fractions act as the driving signal for root architectural responses, and whether such root-soil spatiotemporal coupling can sustain post-anthesis P uptake, yield formation, and P-use efficiency under reduced-P conditions. Therefore, this study aimed to: (1) Quantify how the integrated strategy of γ-PGA combined with banded deep placement reshapes the vertical distribution of soil P fractions in calcareous soils; (2) Clarify how changes in subsoil P availability drive root morphological and architectural responses, particularly fractal characteristics and topological traits; (3) Evaluate how the resulting root-soil spatial coupling regulates P accumulation, yield formation, and P-use efficiency in drip-irrigated maize. The findings will provide a scientific basis for sustainable P management in intensive agriculture across arid regions worldwide.

Materials and methods

Experimental site

This study was conducted from 2024 to 2025 at the Xinjiang Academy of Agricultural and Reclamation Science (Shihezi, Xinjiang, 44°18 N, 86°03E). The study area has a typical arid to semiarid continental climate, characterized by scarce precipitation and abundant sunlight and heat, with an average annual temperature of 8.5-11.8 °C, average annual precipitation of 236.2 mm, and average annual evaporation of approximately 1200 mm. The experimental soil was a calcareous soil, and its physical and chemical properties are listed in Table 1. During the entire crop growth period in 2024 and 2025,

the total precipitation amounted to 178.9 mm and 142.3 mm, respectively, with 12 and 10 effective rainfall events (> 5 mm), respectively, while the average daily maximum temperature was 31.9 °C and 28.5 °C, respectively, and the average daily minimum temperature was 3.14 °C and 2.7 °C, respectively (Fig.1).

Table 1 Physicochemical properties of soil before sowing

Soil depth (cm)	PH	SOM ($g \cdot kg^{-1}$)	AP ($mg \cdot kg^{-1}$)	AK ($mg \cdot kg^{-1}$)	TN ($g \cdot kg^{-1}$)	TP ($g \cdot kg^{-1}$)
0-10	8.32	15.79	17.69	256.67	0.55	0.89
10-20	8.31	15.29	14.32	284.00	0.58	0.93
20-40	8.26	15.06	12.38	215.67	0.47	0.85
40-60	8.50	7.37	6.13	143.33	0.32	0.68

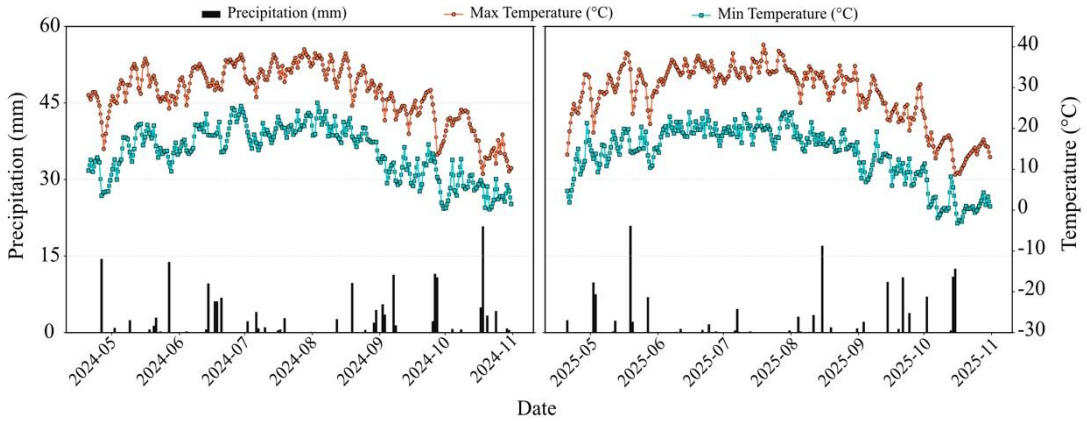

Fig.1. Maximum temperature, minimum temperature, and precipitation during the maize growing seasons in 2024 and 2025

Experimental design

The primary objective of this study is to validate the practical effectiveness of an integrated phosphorus management technology for drip-irrigated maize fields in calcareous soils. The experiment was arranged as a two-factor randomized complete block design with three replicates. The two experimental factors were maize cultivar

and P management strategy. Two maize cultivars were used: Xianyu 335 (a widely adapted cultivar, XY335) and Denghai 550 (a high-yielding cultivar in Xinjiang, DH550). Five P management treatments were established: no P application (P0); conventional P application ((65.5 kg P ha^{-1}, 30% diammonium phosphate (DAP) basal application+70% monoammonium phosphate (MAP) topdressing, P1, CK); 20% P reduction (52.4 kg P ha^{-1}, 30% DAP basal + 50% MAP topdressing, P2); 20% P reduction (52.4 kg P ha^{-1} +γ-PGA (30 kg·ha^{-1}, purity≥90%) +, applied with topdressing fertilizer at jointing stage, via broadcast application,P3); and 20% P reduction (52.4 kg P ha^{-1} +γ-PGA (30 kg·ha^{-1}, purity≥90%) +10 cm banded deep placement (DAP side-banded at 5 cm from the seed row and 10 cm soil depth during sowing), P4).

Each subplot measured 75 m^2, with three replicates. Maize was grown under plastic film-mulched drip irrigation, with a film width of 1.45 m and a planting configuration of four rows and two drip lines per film strip. The planting belt width was 1.65 m, plant spacing was 20 cm, and wide-narrow row spacing was arranged as 50+30 cm (Fig.2). A precision seeder was used to simultaneously lay the drip tapes, apply the plastic film mulch, sow the seeds, and perform banded deep fertilization in a single pass. The system was equipped with inline flat-emitter drip tapes with an emitter spacing of 20 cm, operating at a pressure of 0.2 MPa with a flow rate of 2.3 $L \cdot h^{-1}$. Groundwater from a well was used for irrigation, and the applied volume was precisely monitored using independent water meters. Over the entire growing season, a total irrigation volume of 5100 $m^3 \cdot hm^{-2}$ was applied across nine irrigation events.

The fertilizers used were urea (N ≥ 46.4%), potassium sulfate (K ≥ 42.3%), and

the fertilizer additive γ-polyglutamic acid, all applied through fertigation. Phosphorus fertilizers consisted of monoammonium phosphate (N ≥ 12%, P ≥ 26.6%) and diammonium phosphate (N ≥ 18%, P ≥ 20.1%). Of the total P fertilizer, 30% was applied as basal DAP and 70% as topdressed MAP. Topdressing was split across seven growth stages, namely jointing, early flare stage, 10-leaf stage, late flare stage, tasseling, silking, and grain filling, at proportions of 12.5%, 12.5%, 12.5%, 12.5%, 20%, 20%, and 10.0%, respectively. Sowing was conducted on 20 April 2024 and 28 April 2025, and thinning was initiated 7 days after sowing. All other field management practices were consistent with local conventional management.

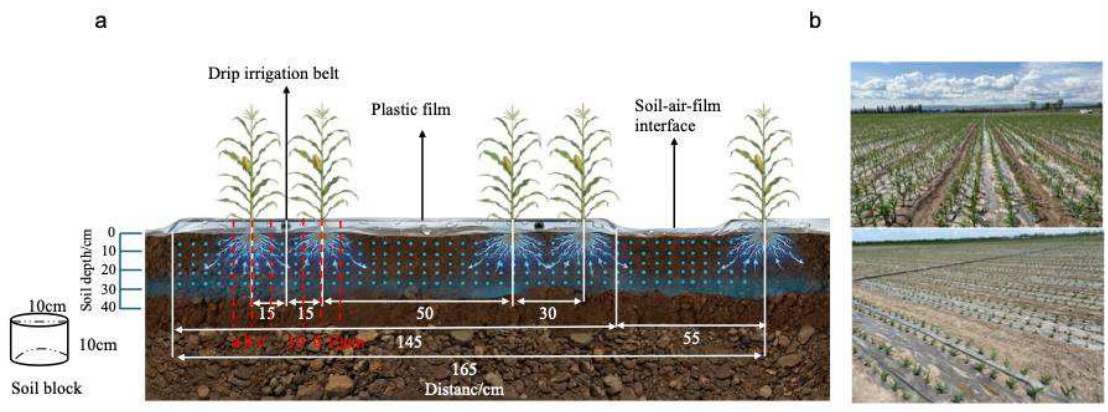

Fig.2. Schematic diagram of cultivation patterns: a, experimental layout; b, field experiment

Samplings and measurements

Yield determination

At maturity, a uniform area of approximately 10 m^2 was selected within each plot for yield determination. Ten fresh ears were sampled using the mean-weight method to evaluate the yield components, including effective ear number, grain number per ear, and 100-grain weight. Grain yield was calculated from the air-dried kernel weight of

179 the sampled 10 ears and adjusted to a standard moisture content of 14%. The calculation
180 formula for phosphorus use efficiency (PUE) and phosphorus partial factor productivity
181 (PFP) is as follows (Hayes et al. 2018):

182 $$PUE = \frac{(PA_p - PA_{np})}{T_{p-apply}} \cdot 100\% \quad (1)$$

183 $$PFP = \frac{Y}{T_{p-apply}} \quad (2)$$

184 Where is the PUE is the Phosphorus use efficiency (%), PA_p is the plant P
185 accumulation under P application ($kg \cdot ha^{-2}$), PA_{np} is the plant P accumulation
186 without P application ($kg \cdot ha^{-2}$), $T_{p-apply}$ is the total P applied, unit: ($kg \cdot ha^{-2}$); Y
187 is the grain yield ($kg \cdot ha^{-2}$).

188 Phosphorus uptake and partitioning

189 At tasseling (74 days after emergence) and maturity (132 days after emergence), five
190 representative maize plants with uniform growth were selected from each plot. After
191 gently cleaning the plants, shoots were cut at the stem base. Samples were first heated
192 at 105°C for 30 min to deactivate enzymes and then oven-dried at 75°C to constant
193 weight for biomass determination on an area basis. Plant organs were subsequently
194 ground to pass a 0.5 mm sieve, digested with H_2SO_4-H_2O_2, and their P concentrations
195 were determined using the molybdenum blue colorimetric method according to Bao
196 (2000).

197 Root morphological traits

198 Vertical root samples were collected at the jointing, tasseling, and grain-filling stages
199 using a soil corer with a diameter of 10 cm. For each treatment, three plants were
200 randomly selected, and the aboveground parts were removed. The stem base was
201 defined as the central sampling point (b), and two additional sampling points (a and c)
202 were established on either side of the plant base, resulting in three horizontal positions
203 in total. In this study, the root system was divided horizontally into a main root zone (-
204 10,10 cm) and lateral root zones (-20, -10 cm) and (10, 20 cm) (Fig. 2). Soil cores were
205 collected at 10-cm intervals downward until no roots were observed. After sampling,
206 weeds, dead roots, and other debris were removed, and the root samples were stored in
207 sealed plastic bags. Roots were then carefully washed with water and spread evenly in
208 an acrylic tray (30 cm × 20 cm) filled to two-thirds with water. Roots were gently
209 separated with forceps to avoid overlap and scanned using an Epson V800 root scanner
210 (Epson Expression, Japan) at 300 dpi to generate black-and-white TIFF images for
211 subsequent analysis. Root traits were analyzed using WinRHIZO (Pro.2020a) software
212 to obtain total root length and the lengths of three root diameter classes: very fine roots
213 ($d \leq 0.5$ mm), fine roots (0.5 mm $< d \leq 1$ mm), and coarse roots ($d > 1$ mm). Root length
214 density (RLD) was calculated as follows:

215 $$RLD = \frac{RL}{SV} \quad (3)$$

216 where RLD is root length density ($m \cdot m^{-3}$), RL is root length (cm), and SV is
217 soil volume (m^3). The soil volume at each depth was 0.785 m^3.

218 Analysis and calculation of root fractal parameters

219 After root morphological sampling, soil profiles were trimmed and an in-house nail

board with 2-cm spacing (ZL201720192129.6; a root sampling device for fibrous-rooted plants; 50 cm × 50 cm, nail length 10 cm) was vertically pressed into the soil to excise intact root-soil blocks. Soil was carefully washed away under running water to obtain complete root samples. The root samples were covered with a glass plate with 2-cm spacing and then inverted to maintain a two-dimensional root plane. The roots were scanned using an Epson 12000 XL scanner at a resolution of 300 dpi to generate digital image files. Fractal analysis of the binary root images was conducted using the self-developed Image J image-processing software based on the box-counting method (Fractal Box Count plugin). In brief, a series of square grids with side lengths r (2, 3, 4, 6, 8, 12, 16, 32, and 64 mm) were superimposed on the two-dimensional binary root image, and the number of occupied squares (N_r) was counted. A linear regression was then fitted with $log_{10}N_r$ as the y-axis and $log_{10}r$ as the x-axis to calculate fractal dimension and fractal abundance as follows:

$$log_{10}Nr = -Dlog_{10}\,r + log_{10}\,K \quad (4)$$

where D is the fractal dimension (FD), represented by the negative slope of the regression line, and lgK is the fractal abundance (FA), represented by the intercept. In general, for plant root systems, 1 < FD < 2; a larger FD indicates a more highly branched and developed root system. FA reflects the spatial extent, density, and resource competitive ability of roots in the growth medium; a larger FA indicates a greater soil exploration volume.

In addition, root length, root surface area, root volume, average diameter, number of root tips, number of branches, number of crossings, average branching angle, and

242 average link length were analyzed. Root tip density (RTI) (Liu et al., 2010) and root
243 branching density (RFI) (Li et al. 2020) were calculated as follows:

244 $$RTI = \frac{RT}{LEN} \quad (5)$$

245 $$RFI = \frac{RF}{LEN} \quad (6)$$

246 where RTI is root tip density, i.e., the number of root tips per unit root length (cm),
247 reflecting the distribution intensity of root tips along the root axis; RFI is root
248 branching density, i.e., the number of branches per unit root length(cm^{-1}), reflecting
249 branching intensity; RT is the number of root tips; LEN is total root length (cm); and
250 RF is the number of root branches.

251 Analysis and calculation of root topological index

252 Root images were analyzed using WinRHIZO (Pro.2020a) software to obtain the
253 number of external links (Magnitude, μ) and the number of links in the longest path of
254 the root system (Altitude, α). The topological index (TI) was calculated according to
255 the classical root topology model proposed by Fitter (1986):

256 $$TI = \frac{lg\alpha}{lg\mu} \quad (7)$$

257 where a TI value approaching 1 indicates that α and μ are approximately equal,
258 meaning fewer root branches and a root system closer to a herringbone branching
259 pattern. By contrast, a TI value approaching 0.5 indicates a greater number of external
260 links (Beidler et al. 2015), a more complex branching structure with more higher-order
261 branches (Lynch 1995; Lynch et al. 2023), and a root system closer to a dichotomous
262 branching pattern (Fig. 3).

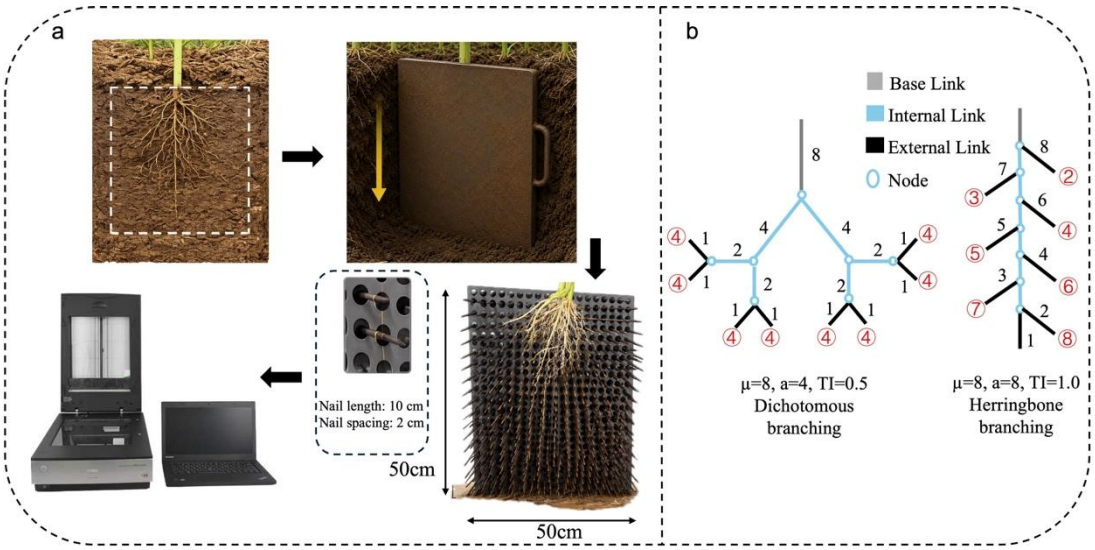

Fig.3. Schematic diagram of root system architecture sampling. a: Sampling of fractal characteristic parameters of root systems, b: schematic diagram of two root system topologies: dichotomous branching (left, TI = 0.5) and herringbone branching (right, TI = 1.0)

Determination of soil physicochemical properties and phosphorus fractions

Soil samples were collected at the jointing, tasseling, and grain-filling stages from the 0-10, 10-20, 20-30, and 30-40 cm soil layers, with three replicates for each treatment. After removing plant residues, stones, and other impurities, soil samples were returned to the laboratory in transparent plastic bags, air-dried under well-ventilated conditions, and ground to pass an 80-mesh sieve. Soil available P was determined by the 0.5 $mol \cdot L^{-1}$ $NaHCO_3$ extraction-molybdenum blue colorimetric method using a continuous-flow analyzer (AA3), and total P was determined by H_2SO_4-$HClO_4$ digestion followed by the molybdenum blue method.

Soil P fractions were determined using the sequential fractionation method originally proposed by Hedley et al. (1982) and later modified by (Moir and Tiessen). Briefly, 0.5 g of soil passed through a 1-mm sieve was sequentially extracted with 30

279 mL deionized water (H_2O), 30 mL 0.5 M $NaHCO_3$ (pH 8.5), 30 mL 0.1 M NaOH, 30
280 mL 1 M dilute HCl, and 10 mL 12 M concentrated HCl (conc. HCl). Residual P was
281 determined after digesting the remaining soil with H_2SO_4-H_2O_2 at 360°C. After each
282 extractant was added, samples were shaken for 16 h at 25°C and 180 oscillations min^{-1}.
283 The suspensions were then centrifuged at 8000 rpm for 4°C and filtered through a 0.45
284 μm cellulose membrane. For inorganic P (Pi) determination, the filtrate was mixed with
285 0.9 M H_2SO_4. For total P (Pt), ammonium persulfate and 0.9 M H_2SO_4 were added to
286 each 2.5 mL aliquot of filtrate, and the mixture was autoclaved after being covered with
287 aluminum foil. The pH of the final Pi and Pt extracts was adjusted using 2,4-
288 dinitrophenol as an indicator. Phosphorus concentration was then determined
289 colorimetrically by the molybdate blue method at 880 nm using a UV
290 spectrophotometer (Murphy and Riley, 1962). Organic P (Po) was calculated as the
291 difference between Pt and Pi.

292 Statistical analyses

293 Analysis of variance and significance testing were conducted using SPSS 16.0 at the
294 0.05 probability level, and mean comparisons were performed using the least significant
295 difference (LSD) test. Year×cultivar×treatment interactions were tested using three-way
296 ANOVA. All statistical analyses and visualizations were conducted in Python 3.12.2,
297 primarily utilizing pandas 2.2.2, numpy 1.26.4, scipy 1.13.1, scikit-learn 1.5.1,
298 statsmodels 0.14.2, matplotlib 3.9.2, and seaborn 0.13.2. Correlation heatmaps were
299 generated using Spearman's rank correlation (two-tailed test); Mantel correlation was
300 based on Euclidean distance matrices, with Mantel r calculated as the Pearson

correlation between distance matrices, and significance assessed via permutation testing. Effect model plots employed Pearson correlation coefficients (r), with 95% confidence intervals derived from Fisher's z transformation. Partial least squares path modeling (PLS-PM) was performed using a two-stage PLS-SEM framework: first, candidate indicators were selected based on Spearman correlations; second, latent variable scores were extracted using PLSRegression; finally, standardized OLS regression (via stats models) was used to estimate structural path coefficients (β) and their significance ($P < 0.05$). Model fit was evaluated using the following metrics: Standardized Root Mean Square Residual (SRMR) = 0.068 (< 0.08, acceptable), Goodness of Fit (GoF) = 0.72 (> 0.36, large effect size), and R^2 values for endogenous variables ranging from 0.68 to 0.79.

Results

Effects of integrated phosphorus management strategy of P fertilizer on yield components and phosphorus use efficiency of drip-irrigated maize

Optimized P management strategies significantly affected maize yield and phosphorus use efficiency ($P < 0.05$), with significant year×treatment interactions detected for yield and PUE (Table 2). In terms of yield components, compared with P1, P2 significantly reduced the panicle numbers and grain number per ear by 4.1%-9.1% and 13.9%-18.4%, respectively, resulting in a significant yield reduction of 7.6%-21.5%. P3 alleviated the nutrient deficit caused by reduced P input, and grain yield did not differ significantly from that under P1. In contrast, P4 fully restored effective ear number and grain number

per ear, maintaining yield stability with no significant different from P1 (-6.0% to +11.7%). Between cultivars, DH550 had significantly more grain number per ear than XY335, whereas 100-grain weight did not differ significantly; consequently, grain yield was not significantly different between the two cultivars.

Regarding phosphorus use efficiency, compared with P1, P2 significantly decreased phosphorus use efficiency (PUE) by 28.1%-62.9%. P3 increased PUE by 3.2%-10.7%, whereas P4 increased PUE by 15.6%-27.1% relative to P1 and enhanced PFP by 20.4%-40.7%. At the cultivar level, DH550 exhibited significantly higher PUE than XY335 under both P1 and P4, with increases of 19.5%-35.3%, indicating a greater potential for resource use and ecological adaptation.

Table 2 Effects of integrated phosphorus management strategy on yield components and phosphorus use efficiency of drip-irrigated maize

Year	Treatment	Panicle numbers（$\times10^4$ hm^{-2}）	Grain number per ear	100-grain weight（g）	Yield（$t•hm^{-2}$）	PUE（%）	PFP（$kg•kg^{-1}$）
2024	XY-P0	9.0±0.2b	385.6±46.3c	34.4±0.7a	11.7±0.1c	-	-
	XY-P1	11.0±0.6a	491.8±74.0ab	36.3±0.7a	16.7±0.3a	38.9±4.8b	110.4±1.7b
	XY-P2	10.0±0.4ab	431.1±28.6b	36.8±1.0a	13.2±0.6b	26.2±4.2c	108.5±4.7b
	XY-P3	10.7±0.3a	494.2±69.3ab	35.1±1.1a	15.1±0.0ab	41.0±13.6ab	125.9±0.1ab
	XY-P4	10.9±0.1a	516.7±84.8a	33.3±0.3a	15.7±0.3ab	46.8±1.7a	129.6±2.4a
	DH-P0	10.0±0.1b	441.6±50.8d	34.7±0.4a	10.7±0.2c	-	
	DH-P1	10.5±0.2a	509.1±66.2a	33.8±0.3a	17.6±0.5a	44.8±4.2a	116.5±2.9c
	DH-P2	9.9±0.2b	475.8±49.7c	34.8±0.3a	15.5±0.5bc	27.2±9.1c	145.6±3.6a
	DH-P3	10.0±0.1ab	491.3±65.1b	31.6±0.4a	16.0±0.4ab	40.6±10.2b	131.9±3.4b
	DH-P4	11.2±0.3a	502.7±68.5a	33.0±0.9a	16.7±0.5ab	49.8±3.7a	132±3.4ab
2025	XY-P0	9.7±0.1b	447.0±20.9d	36.8±3.0a	14.5±0.1b	-	-
	XY-P1	10.3±0.4a	619.8±42.2a	38.7±4.5a	19.1±0.7a	28.0±9.7b	127.5±4.6b
	XY-P2	9.8±0.3b	543.6±43.4bc	37.4±2.1a	15.0±0.2ab	21.7±5.1c	125.0±2.0b
	XY-P3	10.2±0.4ab	534.4±57.2c	38.9±2.0a	16.5±0.7ab	31.0±4.7a	137.4±6.2ab
	XY-P4	10.1±0.3ab	604.0±41.8ab	39.1±2.3a	18.4±1.1a	32.7±9.3a	153.3±9.3a
	DH-P0	9.7±0.7b	398.6±44.2d	37.0±3.3a	12.7±0.4c	-	-
	DH-P1	10.3±0.2a	647.0±37.6a	34.5±1.8a	17.1±1.8b	32.6±4.3a	113.9±11.7b

DH-P2	9.9±0.2b	527.8±39.5bc	33.6±1.0a	15.8±1.1b	25.7±4.1b	131.9±8.8bc
DH-P3	10.3±0.3ab	507.8±33.3c	33.5±2.2a	16.7±0.8b	31.1±6.8a	139.3±6.3ab
DH-P4	11.1±0.6a	577.6±28.0b	34.6±1.9a	19.1±1.2a	37.2±4.0a	159.5±10.0a
ANOVA						
Cultivar (C)	*	***	NS	NS	*	NS
Treatment(T)	**	***	NS	NS	**	***
C×T	**	NS	*	**	**	***

Note: XY: XY335, DH: DH550. P0; P1: conventional P application (CK); P2: 20% P reduction; P3: 20% P reduction +γ-PGA; and P4: 20% P reduction + banded deep placement + γ-PGA. Different letters indicate significant differences among treatments at the 5% level. NS, *, **, *** indicate non-significant or significant at 0.05, 0.01 or 0.001 level, respectively. The same as below.

Effects of integrated phosphorus management strategy of P fertilizer on phosphorus accumulation and translocation in drip-irrigated maize

Optimized P management significantly regulated P accumulation and partitioning in drip-irrigated maize ($P < 0.05$) (Fig. 4). At tasseling, compared with P1, P accumulation under P2 and P3 decreased significantly by 23.1%-34.7% and 14.5%-24.3%, respectively, whereas no significant difference was observed under P4. At maturity, post-anthesis P accumulation under P2 decreased significantly by 30.5%-60.3% relative to P1, and total P accumulation declined by 18.5%-32.0%. Under P3, total P accumulation at maturity was still 8.5%-12.4% lower than under P1. By contrast, P4 increased P accumulation at tasseling and maturity by 5.2%-8.4% and 6.3%-11.5%, respectively. In terms of P translocation and contribution ratios, compared with P1, P4 did not significantly affect pre-anthesis P translocation, but significantly increased post-anthesis P accumulation by 15.8%-26.4% and increased the contribution of post-anthesis P to grain by approximately 8.5%-15.2%, thereby reducing dependence on pre-anthesis translocation. At the cultivar level, XY335 exhibited higher P accumulation at tasseling and maturity, as well as greater post-anthesis P accumulation, than DH550,

whereas the pre-anthesis contribution to grain P was lower. Nevertheless, both cultivars responded similarly to the fertilizer treatments, and both achieved the highest post-anthesis P capture and total P accumulation under P4.

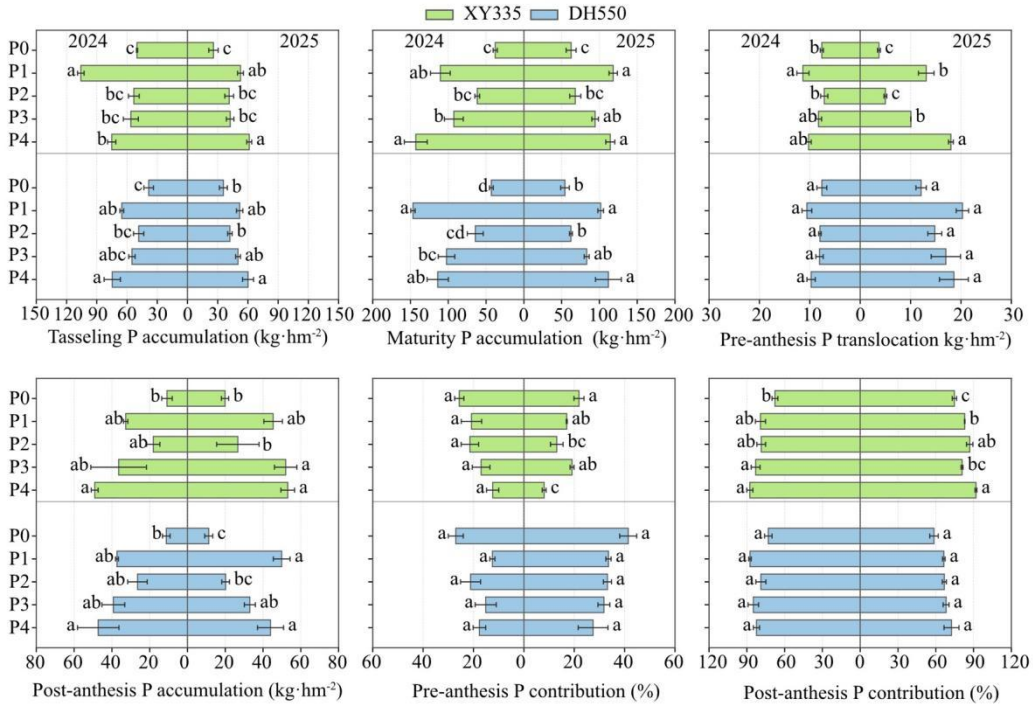

Fig.4. The effect of integrated phosphorus management strategy on the accumulation and transport of phosphorus in drip irrigation maize. P0; P1: conventional P application (CK); P2: 20% P reduction; P3: 20% P reduction +γ-PGA; and P4: 20% P reduction + banded deep placement + γ-PGA. Different letters on the columns indicate significant differences among various phosphorus fertilizer treatments at the 5% level.

Effects of integrated phosphorus management strategy of P fertilizer on root morphological and architectural traits of drip-irrigated maize

For morphological traits (Fig. 5a-k), compared with P1, P2 significantly reduced root length and root surface area by 34.5%-46.7% and 35.6%-43.2%, respectively, and significantly reduced root tip number, branch number, and crossing number by 19.0%-

45.8%, 16.6%-47.0%, and 20.8%-42.3%, respectively. Under P3, root diameter and root volume did not differ significantly from P1, but root tip number and branch number were still 12.0%-14.0% and 8.0%-13.0% lower than under P1. In contrast, P4 significantly increased root length and root volume by 12.3%-28.9% and 5.4%-12.3%, respectively, while average diameter and root surface area did not differ significantly. Moreover, P4 crossing number increasing by 4.8%-20.5%. Root branching angles under P0 and P1 were relatively wide (55°-57°), whereas those under P4 decreased to 48°-49°. Meanwhile, branch density (Fig. 5d) under P2 declined significantly by 6.8%-10.5% compared with P1, whereas P4 increased branch density by 3.5%-8.2%, leading to the formation of a highly compact root framework. DH550 showed significantly greater root morphological traits than XY335, with root length increasing by 16.8%-41.6% across fertilizer treatments.

For root architectural traits (Fig. 5i-o), Compared with P1, P4 increased fractal dimension (FD) and fractal abundance (FA) by 2.4%-5.5% and 1.5%-3.2%, respectively. The topological index (TI) declined by 10.5%-12.5% to 0.50-0.58, and average link length decreased by 25.6%-31.6%, indicating that the root system shifted toward a compact dichotomous branching topology. By contrast, TI and average link length under P2 and P3 did not differ significantly from those under P1. At the cultivar level, XY335 exhibited stronger topological plasticity in response to nutrient conditions; across all P treatments, its TI and average link length remained consistently lower than those of DH550, indicating a greater tendency to develop a denser and more complex root network.

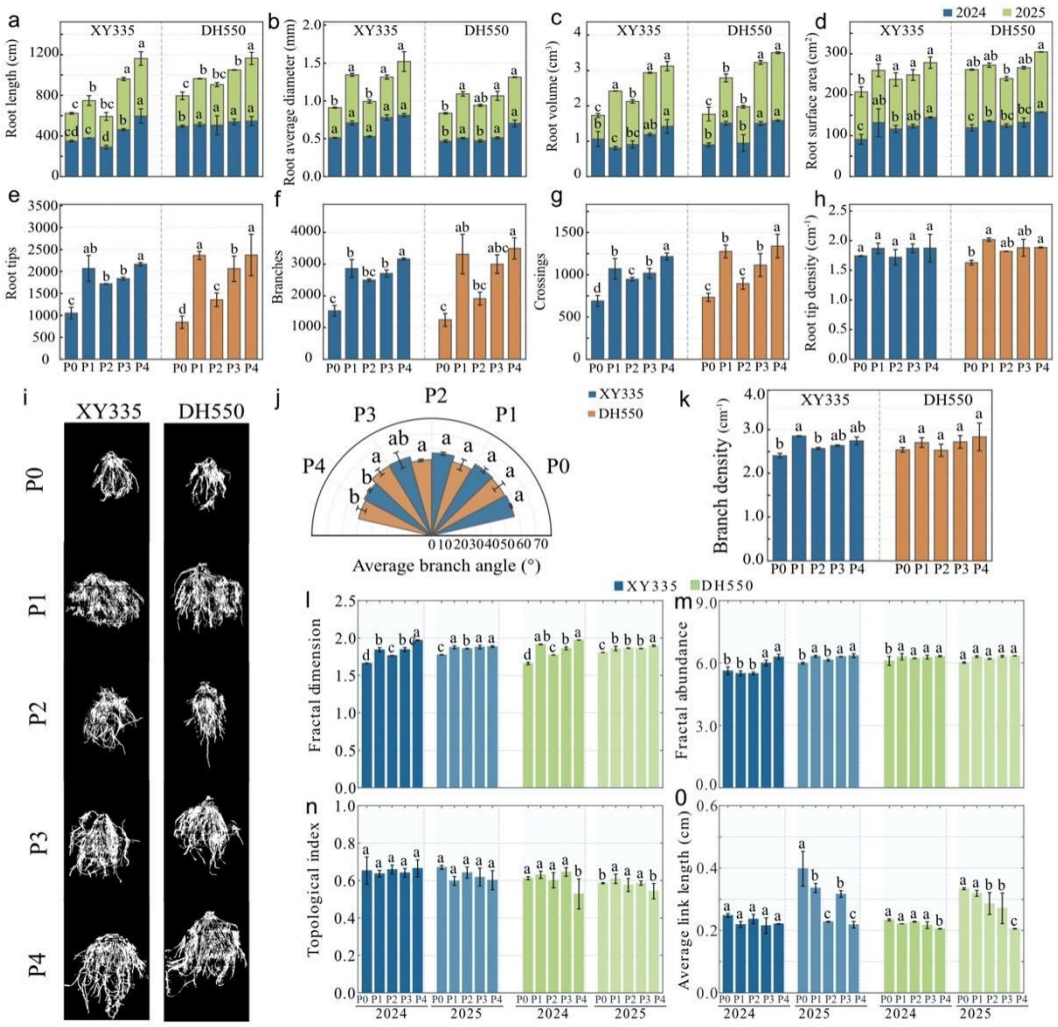

383

384 **Fig.5.** The effect of integrated phosphorus management strategy on the root morphological and architectural traits.

385 P0; P1: conventional P application (CK); P2: 20% P reduction; P3: 20% P reduction +γ-PGA; and P4: 20% P

386 reduction + banded deep placement + γ-PGA. a-h, j-k: Root morphology indices; i: Binary root images; l-o: Root

387 architecture indices. Different letters indicate significant differences at $P < 0.05$.

388 Effects of integrated phosphorus management strategy of P fertilizer on the

389 spatiotemporal distribution of root length density in drip-irrigated maize

390 Root length density (RLD) of different diameter classes showed a unimodal pattern

391 over the growing season, peaking at tasseling (VT). Very fine roots (< 0.5 mm)

392 constituted the major fraction of total RLD, accounting for 56.1%-62.3% (Fig. 6a),

followed by roots of 0.5-1 mm, whereas coarse roots (> 1 mm) contributed the least. Compared with P1, P2 significantly reduced RLD at VT by 22.5%-34.2%, and P3 reduced it by 12.8%-18.5%. In contrast, P4 increased total RLD by 15.6%-28.4% and greatly promoted the proliferation of very fine roots. At the cultivar level, under P application treatments, RLD in DH550 was 15.0%-30.7% higher than that in XY335, with a stronger response particularly in the expansion of very fine roots.

RLD decreased progressively with soil depth (Fig. 6b). In the main root zone (-10, 10 cm), compared with P1, RLD under P2 and P3 decreased by 32.1%-79.5% and 7.3%-46.3%, respectively, whereas no significant difference was observed under P4. In the lateral root zones (-20, -10 cm and 10, 20 cm), P2 reduced RLD by 50.5%-82.1% and 31.4%-68.3%, respectively, whereas P4 significantly increased RLD and promoted root expansion toward the (10, 20 cm) zone, with increases of 19.1%-44.5% relative to P1. Fertilization strategy had contrasting effects on shallow (0-20) cm and deep (20-40) cm root distribution. In the 0-20 cm layer, RLD under P2 and P3 was 48.6%-61.2% and 25.2%-51.2% lower than under P1, respectively, whereas P4 showed no significant difference. In the 20-40 cm layer, both P2 and P3 reduced RLD, whereas P4 increased RLD by 4.4%-38.8% relative to P1.

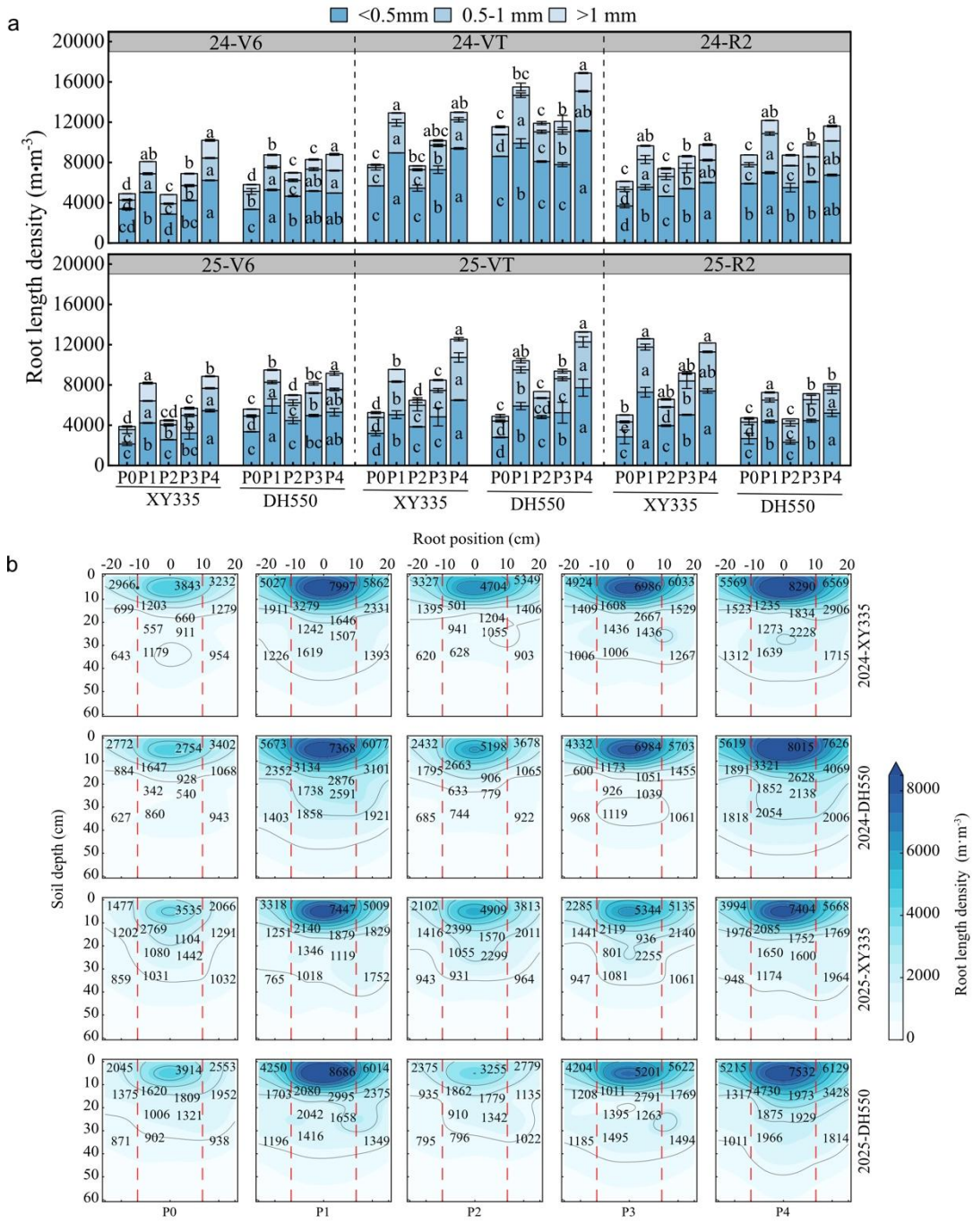

410

411 **Fig.6.** Effects of integrated phosphorus management strategy on the root's spatiotemporal distribution. P0; P1:

412 conventional P application (CK); P2: 20% P reduction; P3: 20% P reduction +γ-PGA; and P4: 20% P reduction +

413 banded deep placement + γ-PGA. a: Root length density of different diameter classes, b: Spatial and temporal

414 distribution characteristics of root length density. V6: jointing stage, VT: Tasseling stage, R2: grain filling stage.

415 Effects of integrated phosphorus management strategy of P fertilizer on soil phosphorus

fractions and phosphorus distribution

Total soil P and available P both declined with increasing soil depth and as the growing season progressed (Fig. 7a-f). Compared with P1, P2 reduced total P and available P throughout the entire growth period. At tasseling, total P and available P in the 0-10 cm layer under P2 were 22.7% and 43.8% lower, respectively, than under P1, whereas P3 showed a significant reduction of 12.5%. Under P4, total P at all growth stages did not differ significantly from that under P1. Available P in the 0-10 cm layer under P4 was 7.8%-9.6% lower than under P1, although the difference was not significant, whereas in the 30-40 cm layer it increased significantly by 31.2%-38.5%, reaching 24.29-26.0 $mg \cdot kg^{-1}$.

Soil phosphorus fraction concentrations gradually decreased with increasing soil depth. Compared to P1, active phosphorus fractions ($NaHCO_3$-Po and NaOH-Pi) and inactive phosphorus (d. HCl-P, c. HCl-Pi) significantly decreased in P2; in P3, active phosphorus fractions significantly decreased ($NaHCO_3$-Po decreased by 32.4% in the 20-30 cm layer, NaOH-Pi decreased by 13.8-20.8% in the 10-30 cm layer), while inactive phosphorus showed significant reductions—d. HCl-P decreased by 9.4-13.7% in the 10-40 cm layer and c. HCl-Po decreased by 25.5-28.8% in the 10-30 cm layer. In P4, $NaHCO_3$-Po increased by 40.9% and 73.9% in the 0-10 cm and 20-30 cm layers, respectively; Resin-P increased by 34.9% in the 30-40 cm layer; however, inactive phosphorus fractions significantly declined (d. HCl-P decreased by 6.4-19.8% across all layers, c. HCl-Pi dropped by 24.2% in the 0-10 cm layer, and c. HCl-Po reduced by

25.7-33.2% in the 10-30 cm layer). In the 30-40 cm soil layer, Resin-P and NaOH-Pi increased by 34.9% and 6.7%, respectively; d. HCl-P, c. HCl-Pi, and Residual-P significantly declined by 13.5%, 26.2%, and 12.2%, respectively.

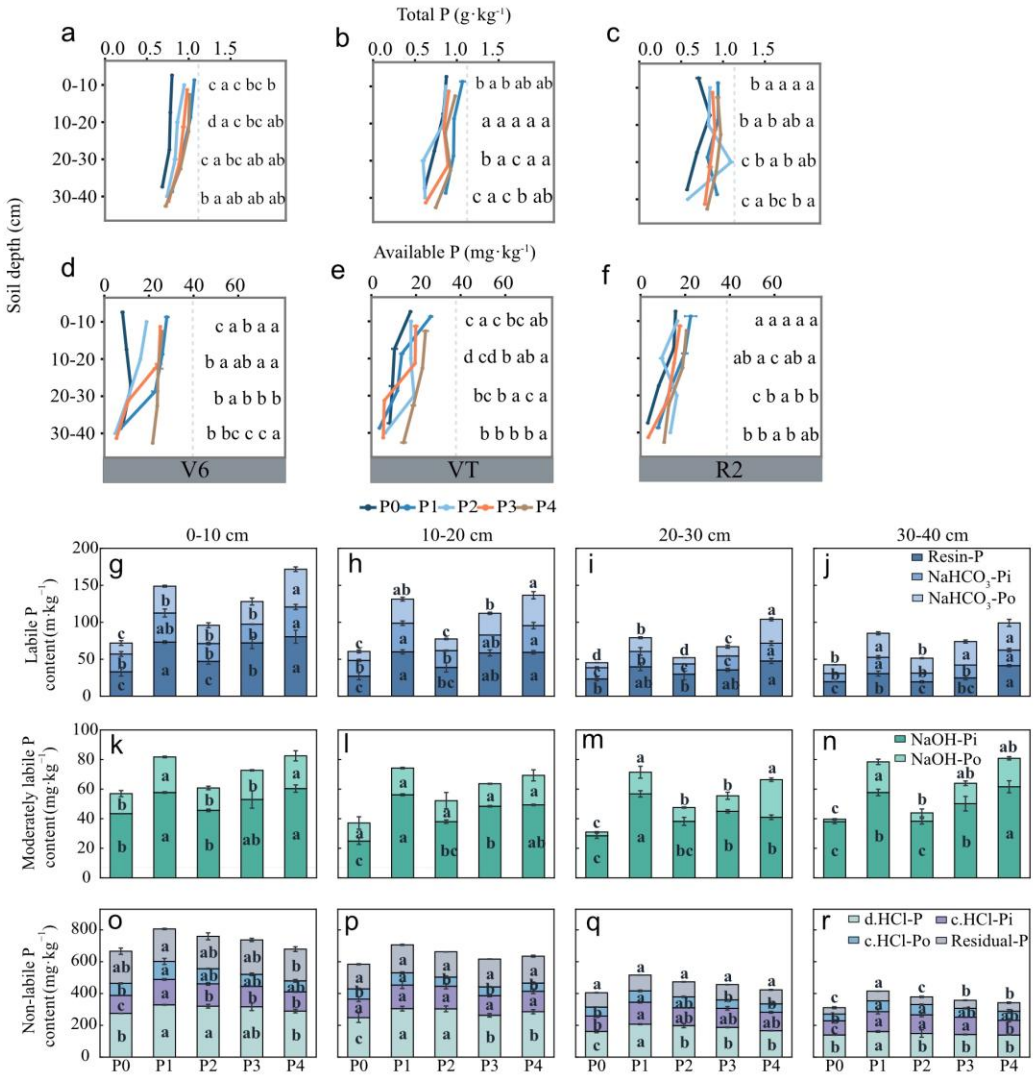

Fig.7. The effect of integrated phosphorus management strategy on soil phosphorus fractions and vertical distribution. P0; P1: conventional P application (CK); P2: 20% P reduction; P3: 20% P reduction +γ-PGA; and P4: 20% P reduction + banded deep placement + γ-PGA. (a-c) Total P content at jointing stage, Tasseling stage and grain filling stage. (d-f) Available phosphorus content at different growth stage. (g-j): Labile P content at 0-40 cm during the tasseling stage. (k-n) Moderately labile P content. (o-r): Non-labile P content.

446 Effects of integrated phosphorus management strategy of P fertilizer on apparent
447 phosphorus balance and surplus rate

448 In terms of P output (Table 3), optimized P management significantly affected maize P
449 uptake. Compared with P1, P uptake under P2 and P3 decreased significantly by 22.6%-
450 44.6% and 3.0%-14.7%, respectively, whereas no significant difference was observed
451 under P4 (ranging from -5.0% to +1.9%). With respect to apparent P balance and surplus
452 rate, P0 showed clear P deficiency, with apparent balance values ranging from -71.1 to
453 -42.2 kg·hm^{-2}. Compared with P1, reduced P uptake under P2 led to a surplus rate
454 exceeding 38%. By contrast, P4 reduced environmental redundancy, with apparent P
455 balance declining by 51.3%-64.8% relative to P1 and the P surplus rate maintained
456 within 12.5%-21.0%. At the cultivar level, DH550 exhibited lower apparent P balance
457 than XY335, and its surplus rate was 11.0%-18.6% lower, indicating stronger nutrient
458 conversion efficiency and a lower potential risk of non-point source pollution.

Table 3 Effects of integrated phosphorus management strategy of P fertilizer on apparent phosphorus balance and surplus rate

Year	Treatment	XY335			DH550		
		Output (kg·hm^{-2})	P apparent balance (kg·hm^{-2})	Surplus rate (%)	Output (kg·hm^{-2})	P apparent balance (kg·hm^{-2})	Surplus rate (%)
2024	P0	42.2±0.77e	-42.2±0.77d	-	47.6±2.14d	-47.6±2.14d	-
	P1	100.5±6.57a	49.5±6.57b	49.9±10.25c	115.9±4.42a	34.1±4.42c	29.6±5.01c
	P2	61.6±4.51d	67.4±4.51a	85.8±6.52a	64.2±14.93c	55.8±14.93a	96.1±40.06a
	P3	92.6±17.62b	27.4±17.62b	35.2±29.7c	102.3±15.5b	24.3±10.85b	20.3±20.3c
	P4	102.4±6.51a	21±3.01c	21.0±3.92d	110.1±8.58ab	16.6±4.14c	18.7±2.67d
2025	P0	71.1±10.5d	-71.1±10.5d	-	65.6±3.2d	-65.6±3.2d	-
	P1	113.1±4.6a	36.9±1.3a	32.88±5.89a	110.4±8.1b	39.6±8.1a	36.59±5.5ab
	P2	87.5±9.8d	32.5±9.8a	38.92±0.02a	84.4±5.1cd	35.6±5.1a	42.12±6.55a
	P3	109.7±3.8c	10.3±3.8b	29.52±3.29c	94.2±15.4c	25.8±1.6b	30.63±17.23b
	P4	110.3±0.9b	13.0±3.8c	15.42±1.9c	110.2±6.3a	14.4±1.2c	12.55±1.31c
	ANOVA						

Cultivar (C)	NS	*	*	NS	*	*
Treatment(T)	**	**	**	**	**	**
C×T	NS	**	*	NS	**	*

459 Mechanistic analysis of root-soil spatial coupling driving the coordinated improvement
460 of yield and phosphorus use efficiency

461 Mantel correlation analysis (Fig. 8) showed that NaOH-Pi, fractal dimension (FD),
462 Resin-P, and P accumulation at maturity were significantly and positively correlated
463 with grain yield, whereas d. HCl-P was significantly negatively correlated with yield.
464 Phosphorus use efficiency (PUE) was significantly positively correlated with FD, P
465 accumulation at maturity, post-anthesis P accumulation, and NaOH-Po, but negatively
466 correlated with RLD of roots > 1.0 mm in diameter. Apparent phosphorus balance (APB)
467 was significantly positively correlated with fractal abundance (FA), c. HCl-Pi, NaOH-
468 Pi, and P accumulation at maturity.

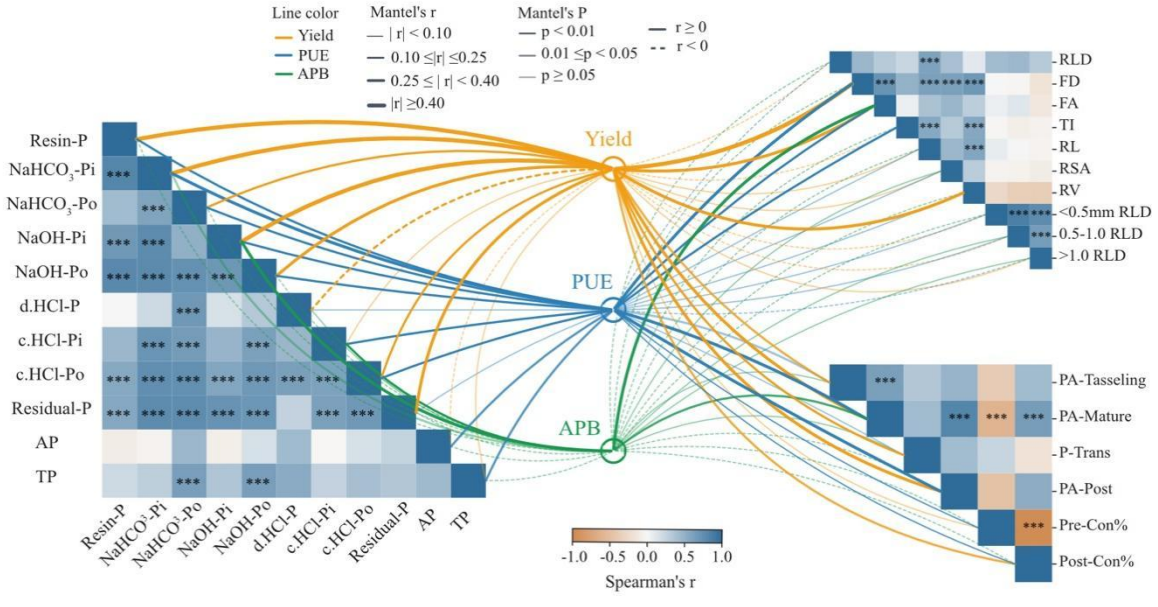

469

470 **Fig.8.** Mantel test evaluates the correlation between soil environmental factors, root system characteristics, plant
471 phosphorus accumulation transport and yield and phosphorus utilization. SOM: Soil Organic Matter, AP: Available
472 Phosphorus, TP: Total Phosphorus, FD: Fractal Dimension, FA: Fractal Abundance, TI: Topological Index, RSA:

Root Surface Area, RV: Root Volume, PA-Tasseling：Tasseling P accumulation, PA-Mature: Maturity P accumulation, P-Trans: Pre-anthesis P translocation, PA-Post: Post-anthesis P accumulation, Pre-Con%: Pre-anthesis P contribution, Post-Con%: Post-anthesis P contribution.

The relative effects model further indicated that soil indicators contributed 31.5% to ear number (Fig.9), among which Resin-P, $NaHCO_3$-Pi, and $NaHCO_3$-Po were significantly positively correlated with ear number, while root architectural traits accounted for 25.6%, with FD and FA showing highly significant positive relationships with ear number ($p < 0.001$). Contributions of P accumulation (28.9%) and soil indicators (27.6%) to grain number per ear were comparable, and both FD and TI were significantly positively correlated with grain number per ear. For grain yield, soil indicators (29.0%) and P accumulation (30.8%) contributed similarly, and Resin-P, $NaHCO_3$-Pi, $NaHCO_3$-Po, as well as P accumulation at maturity (PA-Mature) and pre-anthesis P translocation (P-Trans), were all highly significantly and positively correlated with yield ($p < 0.001$). PUE was jointly dominated by aboveground P accumulation (32.8%) and soil P indicators (27.3%), while root geometric and architectural traits also showed significant relationships. Soil indicators contributed the most to partial factor productivity of phosphorus (PFP, 31.9%), and TI was negatively correlated with PFP.

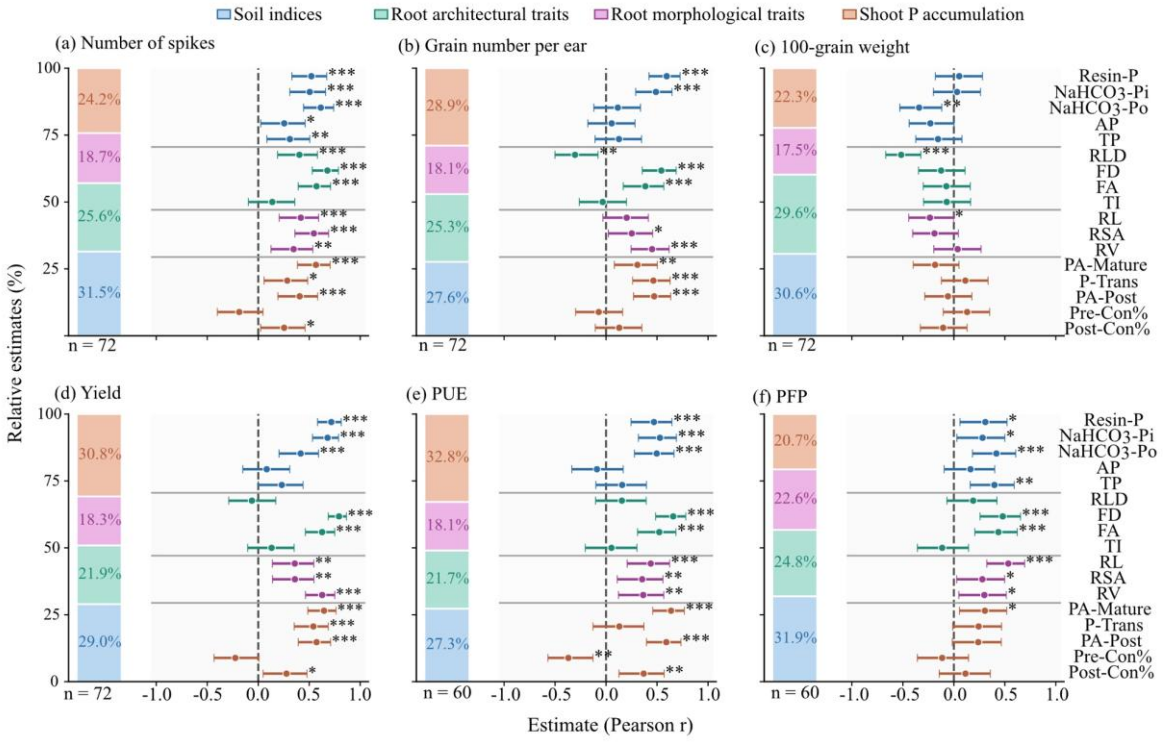

491

492 **Fig.9.** Linear mixed effect model of based on root traits with yield and phosphorus use efficiency. All points represent

493 the variation in effect sizes of different root system indices within the 95% confidence interval; the intersection of

494 error bars with the zero line indicates no significant difference in root system indices with respect to environmental

495 factors. Asterisks (*) indicate the level of significance: * $p < 0.05$, ** $p < 0.01$, *** $p < 0.001$.

496 The partial least squares path model (PLS-PM, Fig. 10) further revealed that

497 NaOH-Po and NaOH-Pi exerted significant positive effects on FD (β = 0.78 and 0.59,

498 respectively); NaOH-Po showed a positive effect on root volume (RV; β = 0.32); and

499 both NaOH-Po and $NaHCO_3$-Pi exerted significant positive effects on FA (β= 0.71 and

500 0.67). FD significantly increased both P accumulation at maturity (β = 0.78) and post-

501 anthesis P accumulation (β = 0.59). Grain yield was well explained by the model (R^2 =

502 0.79), with significant positive effects originating from FD (β = 0.77) and NaOH-Pi (β

503 = 0.76). The explanatory power for PUE was also high (R^2 = 0.68), with significant

504 pathways including a negative effect of FA (β = -0.61) and positive effects of P

accumulation at maturity and NaOH-Pi (β = 0.49 and 0.68, respectively). Overall, FD and NaOH-Pi emerged as key determinants of grain yield, whereas NaOH-Pi and P accumulation at maturity were the major factors regulating phosphorus use efficiency.

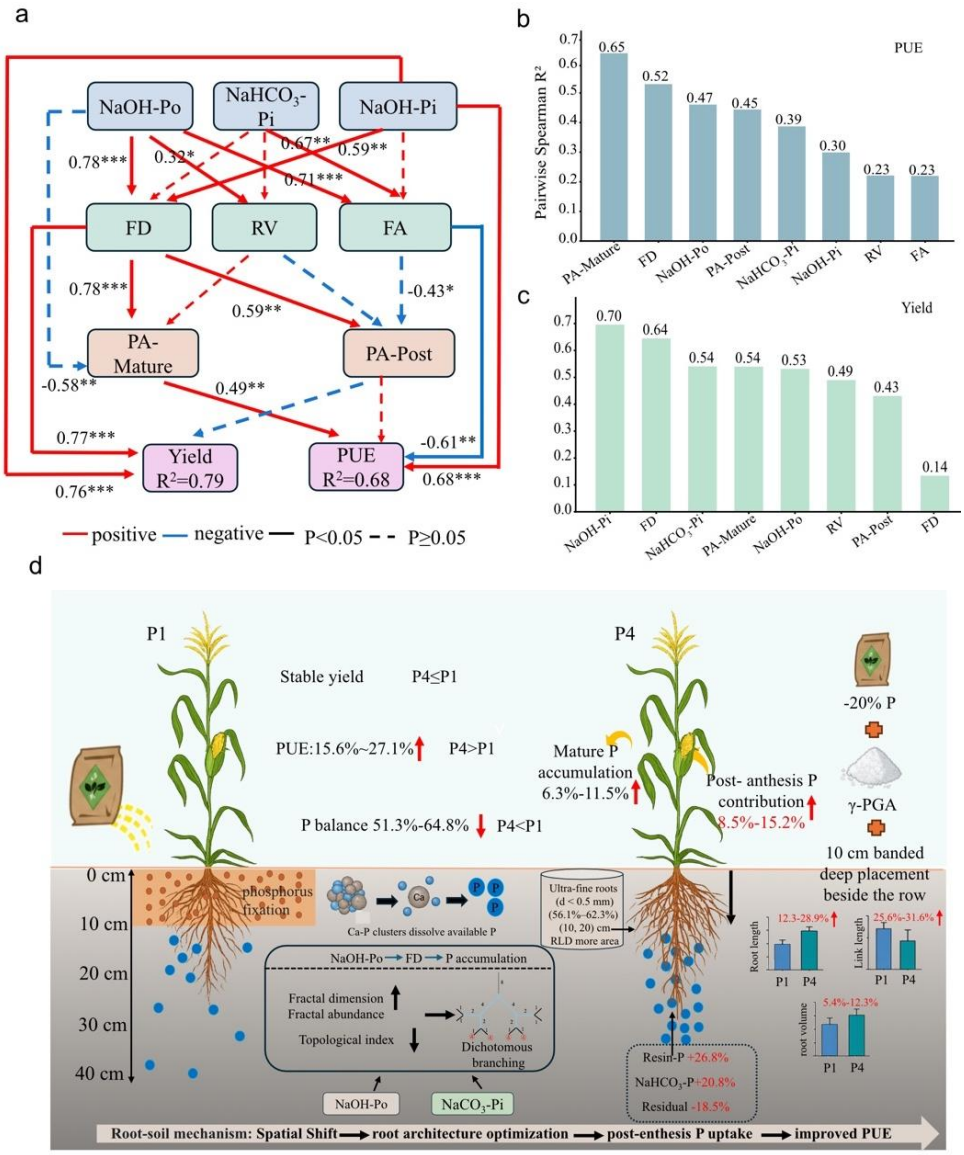

Fig.10. Partial least squares path model（PLS-PM）demonstrates the causal pathways from soil P fractions, root architectural traits, P accumulation, yield, and PUE. a: Structural equation modeling assessing the effects of root-soil interactions on yield and phosphorus fertilizer use efficiency; b: Proportion of variance explained (R^2) by each latent variable in phosphorus use efficiency; c: Proportion of variance explained (R^2) by each latent variable in yield; d: Schematic diagram illustrating fertilizer management strategies aimed at improving root traits and active

phosphorus fractions to enhance nutrient accumulation in maize. The red line indicates a positive effect, and the blue line indicates a negative effect; solid lines represent $p < 0.05$, and dashed lines represent $p \geq 0.05$; Numbers adjacent to arrows represent standardized path coefficients (β). Model fit: SRMR = 0.068, GoF = 0.72, R^2(Yield) = 0.79, R^2(PUE) = 0.68.

Discussion

Integrated phosphorus management strategy enhances Post-anthesis P uptake and maintains yield and PUE under reduced p input

Phosphorus (P) accumulation in maize grains depends largely on the translocation of P stored pre-anthesis, and the export of P from vegetative organs to the grains serves as a crucial source for maintaining grain filling. In this study, compared with conventional P application (P1), a 20% reduction in P application (P2) decreased P accumulation at the tasseling and maturity stages, as well as post-anthesis. The pre-anthesis P translocation amount and its contribution to the grains failed to effectively compensate for the deficiency in post-anthesis P uptake (Fig. 4), resulting in a decline in yield and phosphorus use efficiency (PUE). When the reduced P application was combined with γ-PGA (P3), the yield showed no significant difference from that of P1, and the partial factor productivity of applied P was improved. However, relying solely on biochemical regulation is constrained by the interception space of the surface soil. Under the alternating wet and dry conditions typical of drip irrigation, the activated P in the topsoil is highly susceptible to re-fixation, making it difficult to meet the nutrient demands during the mid-to-late growth stages. Previous studies have indicated that when the

root-zone nutrient supply is sufficient during the later growth stages, the contribution of post-anthesis P uptake to grain formation is significantly enhanced (Wang et al. 2020b; Yang et al. 2025). Consistent with these findings, P4 improved P accumulation during the post-anthesis and maturity stages, increasing the contribution rate of post-anthesis P to the grains by 8.5%-15.2% compared to P1, and significantly increasing PUE by 15.6%-27.1%.

Compared to other phosphorus reduction technologies reported in recent literature, the comprehensive phosphorus management strategy proposed in this study demonstrates significant advantages. Biochar application typically increases PUE by 8%-15% (Zhang et al., 2025), optimized fertigation can enhance it by 10%-20% (Bian et al. 2024), and straw return combined with optimized phosphorus fertilization can improve it by 14.0%-18.4%(Yang et al. 2017). In contrast, the P4 treatment-maintained yield stability while reducing phosphorus application by 20%, achieving a PUE increase of 15.6%-27.1%. Furthermore, the apparent phosphorus balance was reduced by 51.3%-64.8%(Gong et al. 2025b).

Integrated phosphorus management optimizes root architecture and improves P acquisition under reduced P input

Root systems exhibit strong plasticity in response to heterogeneous nutrient environments, and their spatial distribution and architectural characteristics are crucial in determining P acquisition efficiency (Miguel et al. 2015; Lynch et al. 2023; Tang et al. 2023). A key finding of this study is that under reduced P conditions, the root

response is not merely manifested in changes to root length or root mass but is further reflected in the optimization of spatial root architecture. Compared with P1, the P2 treatment decreased root length, root surface area, number of root tips, number of branches, and number of crossings by 34.5%-46.7%, 35.6%-43.2%, 19.0%-45.8%, 16.6%-47.0%, and 20.8%-42.3%, respectively (Fig. 5), which significantly weakened the exploration capacity of maize roots for soil resources. There was no significant difference in root diameter and root volume between P3 and P1; however, the number of root tips and branches in P3 remained lower than those in P1, and the topological index (TI) and average link length did not show significant improvement. This indicates that γ-PGA regulation primarily alleviated the decline in quantitative root traits but was insufficient to reshape the spatial root architecture. P4 not only increased root length, root volume, and the number of crossings, but also enhanced the fractal dimension and fractal abundance. It reduced the TI to 0.50-0.58 and shortened the average link length by 25.6%-31.6%, facilitating the transformation of the root system into a compact dichotomous branching structure. This is likely because the synergistic effect of deep placement and γ-PGA improved the P supply environment in the root zone, enabling the root system to form a high-density branching network and a larger root-soil contact interface with limited carbon investment (Fitter et al., 1991; Lynch, 1995; Sun et al., 2022), thereby enhancing the spatial capture capacity for low-mobility P resources(Fitter et al. 1991; Lynch 1995; Sun et al. 2022), thereby enhancing the spatial capture capacity for low-mobility P resources. Most previous studies have considered root morphological changes as a result of improved soil nutrient conditions (He et al.

578 2024; Zhou et al. 2026). In this study, the contributions of root architecture to yield and
579 PUE reached 21.7% and 20.4%, respectively (Fig. 9), indicating that highly efficient P
580 acquisition in maize does not simply rely on an increase in root quantity, but rather on
581 the optimization of spatial root configuration, branching structure, and the absorption
582 interface.

583 Root functions vary across different diameter classes; very fine roots (<0.5 mm)
584 serve as the primary functional roots for P acquisition due to their large specific surface
585 area and high metabolic activity (Postma et al. 2014; Guo and York 2019; Lugli et al.
586 2020).In the present study, the P4 treatment increased the proportion of very fine roots
587 and the root length density (RLD) in the 30-40 cm soil layer (Fig. 6). This may be
588 attributed to the placement of P fertilizer 5 cm away from the seed row and at a depth
589 of 10 cm, which is closer to the root expansion zone of the seedlings. Such placement
590 enhances early root-fertilizer contact efficiency and creates localized nutrient
591 heterogeneity, thereby influencing the subsequent spatial distribution of the roots(Ma
592 et al. 2021; Zhou et al. 2025); Previous studies have shown that deep placement at 15
593 cm increases root dry weight and root length in the 20-60 cm soil layer by an average
594 of 23.2%, while combining deep placement with fertigation via drip irrigation
595 significantly promotes root growth in the 10-40 cm layer and enhances root activity
596 within the 0-60 cm profile (Chen et al. 2024b; He et al. 2024). The co-application of γ-
597 PGA, which is rich in carboxyl functional groups, likely interacts with Ca^{2+} to mitigate
598 P fixation and facilitate the transformation of less available P into more labile forms,
599 thereby prolonging the duration of effective P supply in the root zone (Liang and Shi

2021; Zhu et al. 2026; Liu et al. 2026). Mantel tests revealed that Resin-P, $NaHCO_3$-Pi, and NaOH-Po were all significantly correlated with crop yield and PUE (Fig. 8), indicating that efficient P acquisition and yield formation primarily depend on the enhancement of labile P pools and the optimization of root architecture.

Furthermore, genetic background is a crucial factor determining differences in root morphology and spatial configuration. Genotypic variations dictate the exploration strategies of roots for soil resources and their level of plasticity, exhibiting distinct nutrient acquisition strategies and environmental adaptability (Postma et al. 2014; Schneider et al. 2020). In this study, the RLD and PUE of the DH550 genotype were 15.0%-30.7% and 19.5%-35.3% higher than those of XY335, respectively. Concurrently, its P surplus rate decreased, and its TI and average link length were reduced, indicating that DH550 achieves high P utilization efficiency through superior resource acquisition capacity and conversion efficiency.

Integrated phosphorus management strategies promote synergistic root-soil P supply by regulating active P distribution

P availability depends on the dynamic equilibrium among active P fractions and their spatial matching with root distribution (Alam et al. 2018; Yang et al. 2021b; Hinsinger). In calcareous soils, phosphate readily binds with Ca^{2+} to form poorly soluble calcium-phosphate compounds, leading to the rapid transformation of applied P into stable forms. In this study, compared to P1, P2 significantly decreased available phosphorus (AP) and active P fractions such as Resin-P across the entire soil profile (Fig. 7). Although

P3 maintained surface AP levels, it did not significantly improve NaOH-Pi/Po, indicating a limited capacity to enhance the moderately active P pool and deep soil P supply, which subsequently led to a decline in P uptake during the late growth stages (Fig. 4). Given the extremely limited diffusion distance of P in calcareous soils (Lombi et al. 2005), the distribution of active P fractions within the effective root absorption zone is particularly critical for P acquisition in maize. P4 maintained total P levels in the 0-10 cm soil layer comparable to those of P1, while increasing Resin-P and $NaHCO_3$-Po in the 30-40 cm layer by 26.8% and 20.8%, respectively. This translated into a superior root architecture and higher P use efficiency, demonstrating that the integrated P management strategy optimized the spatial allocation of P fractions within the root zone profile. These results reflect the holistic regulation of the comprehensive P management strategy on the P supply environment in the root zone, the transformation processes of active P, and the spatial distribution of roots. Partial least squares path modeling (PLS-PM) further demonstrated that active P fractions induced the optimization of the spatial root architecture, thereby promoting synergistic root-soil P supply. This enhanced Post-anthesis P uptake, ultimately achieving stable yields and improved efficiency at maturity (Fig. 10).

In summary, under reduced P conditions, integrated phosphorus management strategies enhance PUE in maize primarily through two interconnected processes. First, they optimize the P supply environment in the root zone by regulating the composition of different active P pools, thereby ensuring a stable P supply during the reproductive stage. Second, they promote the optimization of root system architecture and enhance

Post-anthesis P uptake capacity, which consequently maintains P accumulation, yield, and PUE at maturity. This study reveals the holistic regulatory effects of integrated phosphorus optimization strategies on the root-soil system, rather than the independent contributions of isolated measures. Future research urgently needs to incorporate isotope tracing techniques (^{32}P) to quantify the availability of different phosphorus sources. Furthermore, utilizing metagenomics and rhizosphere metabolomics, subsequent studies should deeply elucidate the underlying biological mechanisms of efficient phosphorus utilization from a plant-soil-microbe perspective.

Conclusion

This study demonstrates that merely reducing phosphorus (P) input in calcareous soils is insufficient to maintain P uptake and yield formation in maize. In contrast, an integrated management strategy combining deep placement with γ-PGA maintained grain yield and enhanced PUE despite a 20% reduction in P application. The superior performance of this integrated strategy can be attributed to two synergistic response mechanisms. First, by regulating the composition and spatial distribution of the active P pool, it optimized the P supply environment within the root zone, thereby sustaining high P availability during the reproductive growth stage. Second, the strategy facilitated the optimization of root system architecture, which enhanced soil exploration capacity and sustained continuous P uptake after anthesis. These synergistic changes strengthened the spatiotemporal coordination between soil P supply and plant P uptake, providing a robust explanation for the improved PUE under reduced P input conditions.

In conclusion, achieving efficient P management in calcareous soils relies not only on increasing the available P content in the soil but also on enhancing the coordination between soil P dynamics and root foraging strategies. These findings provide both a technical reference and a mechanistic basis for management practices aimed at reducing P input and increasing efficiency in drip-irrigated maize in calcareous soils.

Author contributions

Qingyun Tang: Conceptualization, Data curation, Formal analysis, Writing - original draft, Writing - review & editing. **Guojiang Yang:** Formal analysis, Writing - review & editing. **Zhong Zheng:** Formal analysis, Project administration. **Jiahui Hao:** Data curation, Formal analysis, Investigation. **Xin Zhu:** Data curation, Formal analysis, Investigation. **Kexin Xie:** Data curation, Conceptualization. **Zhijian Gao:** Methodology, Investigation. **Yali Zhang:** Formal analysis, Writing original draft, Writing - review & editing. **Guodong Wang:** Project administration, Validation, Writing original draft, Writing - review & editing. **Yuxiang Li:** Writing original draft, Writing - review & editing.

Funding

This work was supported by the Tianshan Talent Science and Technology Innovation Team Program (2024TSYCTD0019), the Agricultural Science and Technology Major Project and the Earmarked Fund (XJARS-02-14).

Data availability

Data will be made available on request.

Declarations

Competing Interest

The authors declare that they have no known competing financial interests or personal relationships that could have appeared to influence the work reported in this paper.

References

Alam MdK, Bell RW, Salahin N, et al (2018) Banding of fertilizer improves phosphorus acquisition and yield of zero tillage maize by concentrating phosphorus in surface soil. Sustainability 10:3234. https://doi.org/10.3390/su10093234

Beidler KV, Taylor BN, Strand AE, et al (2015) Changes in root architecture under elevated concentrations of CO_2 and nitrogen reflect alternate soil exploration strategies. New Phytol 205:1153-1163. https://doi.org/10.1111/nph.13123

Bian Q, Dong Z, Fu Y, et al (2024) Optimizing irrigation strategies to improve yield and water use efficiency of drip-irrigated maize in southern xinjiang. Plants 13:3492. https://doi.org/10.3390/plants13243492

Chen X, Ren H, Zhang J, et al (2024a) Deep phosphorus fertilizer placement increases maize productivity by improving root-shoot coordination and photosynthetic performance. Soil Tillage Res 235:105915. https://doi.org/10.1016/j.still.2023.105915

Chen X, Ren H, Zhang J, et al (2024b) Deep phosphorus fertilizer placement increases maize productivity by improving root-shoot coordination and photosynthetic performance. Soil Tillage Res 235:105915. https://doi.org/10.1016/j.still.2023.105915

Chun HC, Lee S, Choi YD, et al (2021) Effects of drought stress on root morphology and spatial distribution of soybean and adzuki bean. J Integr Agric 20:2639-2651. https://doi.org/10.1016/S2095-3119(20)63560-2

Fitter AH (1986) The topology and geometry of plant root systems: influence of watering rate on root system topology in trifolium pratense. Ann Bot 58:91-101. https://doi.org/10.1093/oxfordjournals.aob.a087191

Fitter AH, Stickland TR, Harvey ML, Wilson GW (1991) Architectural analysis of plant root systems 1. Architectural correlates of exploitation efficiency. New Phytol 118:375-382. https://doi.org/10.1111/j.1469-8137.1991.tb00018.x

714 Gong H, Yin Y, Chen Z, et al (2025a) A dynamic optimization of soil phosphorus status approach
715 could reduce phosphorus fertilizer use by half in China. Nat Commun 16:976-986.
716 https://doi.org/10.1038/s41467-025-56178-1

717 Gong P, Li Y, Liu H, et al (2025b) Root zone infiltration irrigation affects plastic root developmental
718 traits of fruit trees and root zone habitat in saline-alkali soil. Agric Water Manag
719 319:109802. https://doi.org/10.1016/j.agwat.2025.109802

720 Guo H, York LM (2019) Maize with fewer nodal roots allocates mass to more lateral and deep roots
721 that improve nitrogen uptake and shoot growth. J Exp Bot 70:5299-5309.
722 https://doi.org/10.1093/jxb/erz258

723 Guo H-L, Tian M-Z, Ri X, Chen Y-F (2025) Phosphorus acquisition, translocation, and
724 redistribution in maize. J Genet Genomics 52:287-296.
725 https://doi.org/10.1016/j.jgg.2024.09.018

726 Guo Y, Wang Z, Li J (2024) Effects of phosphorus fertilizer type and dripline depth on root and soil
727 nutrient distribution, nutrient uptake, and maize yield under subsurface drip fertigation.
728 Field Crops Res 318:109585. https://doi.org/10.1016/j.fcr.2024.109585

729 Hayes PE, Clode PL, Oliveira RS, Lambers H (2018) Proteaceae from phosphorus-impoverished
730 habitats preferentially allocate phosphorus to photosynthetic cells: an adaptation improving
731 phosphorus-use efficiency. Plant Cell Environ 41:605-619.
732 https://doi.org/10.1111/pce.13124

733 He Z, Dang X, Gao G, et al (2024) Integrated deep banding and fertigation of phosphorus improves
734 cotton yield by regulating root spatial distribution and growth. Field Crops Res 318:109604.
735 https://doi.org/10.1016/j.fcr.2024.109604

736 Hedley MJ, Stewart JWB, Chauhan BS (1982) Changes in inorganic and organic soil phosphorus
737 fractions induced by cultivation practices and by laboratory incubations. Soil Sci Soc Am
738 J 46:971-976. https://doi.org/10.2136/sssaj1982.03615995004600050017x

739 Hinsinger P Bioavailability of soil inorganic P in the rhizosphere as affected by root-induced
740 chemical changes: A review. 1-23. https://doi.org/10.1023/A:1013351617532

741 Jiang B, Shen J, Sun M, et al (2021) Soil phosphorus availability and rice phosphorus uptake in
742 paddy fields under various agronomic practices. Pedosphere 31:103-115.
743 https://doi.org/10.1016/S1002-0160(20)60053-4

744 Li J, Zhou M, Zhu J, Xu C (2020) Adaptability response of root architecture of Cotinus coggygria
745 seedlings to soil nutrient stress. J Beijing For Univ 42:65-77

746 Liang J, Shi W (2021) Poly-γ-glutamic acid improves water-stable aggregates, nitrogen and
747 phosphorus uptake efficiency, water-fertilizer productivity, and economic benefit in barren
748 desertified soils of Northwest China. Agric Water Manag 245:106551.
749 https://doi.org/10.1016/j.agwat.2020.106551

750 Liu J, Xiang W, Xu X, et al (2010) Analysis of architecture and functions of fine roots of five
751 subtropical tree species in Huitong, Hunan Province, China. Chin J Plant Ecol 34:938-945.
752 https://doi.org/10.3773/j.issn.1005-264x.2010.08.006

753 Liu M, Zheng J, Wen Y, et al (2026) Poly-γ-glutamic acid improves soil structure to enhance seed
754 cotton yield and fiber quality in arid saline regions. Ind Crops Prod 243:123156.
755 https://doi.org/10.1016/j.indcrop.2026.123156

756 Lombi E, McLaughlin MJ, Johnston C, et al (2005) Mobility, solubility and lability of fluid and
757 granular forms of P fertiliser in calcareous and non-calcareous soils under laboratory
758 conditions. Plant Soil 269:25-34. https://doi.org/10.1007/s11104-004-0558-z

759 Loudari A, Mayane A, Naciri R, et al (2022) Root morphological and anatomical responses to
760 increasing phosphorus concentration of wheat plants grown under salinity. Plant Stress
761 6:100121. https://doi.org/https://doi.org/10.1016/j.stress.2022.100121

762 Lugli LF, Andersen KM, Aragão LEOC, et al (2020) Multiple phosphorus acquisition strategies
763 adopted by fine roots in low-fertility soils in central amazonia. Plant Soil 450:49-63.
764 https://doi.org/10.1007/s11104-019-03963-9

765 Lynch J (1995) Root Architecture and Plant Productivity. Plant Physiol 109:7-13.
766 https://doi.org/10.1104/pp.109.1.7

767 Lynch JP, Galindo-Castañeda T, Schneider HM, et al (2023) Root phenotypes for improved nitrogen
768 capture. Plant Soil 1-55. https://doi.org/10.1007/s11104-023-06301-2

769 Ma Q, Sun L, Tian H, et al (2021) Deep banding of phosphorus and nitrogen enhances rosa
770 multiflora growth and nutrient accumulation by improving root spatial distribution. Sci
771 Hortic 277:109800. https://doi.org/10.1016/j.scienta.2020.109800

772 McDowell RW, Pletnyakov P, Haygarth PM (2024) Phosphorus applications adjusted to optimal
773 crop yields can help sustain global phosphorus reserves. Nat Food 5:332-339.
774 https://doi.org/10.1038/s43016-024-00952-9

775 Miguel MA, Postma JA, Lynch JP (2015) Phene synergism between root hair length and basal root
776 growth angle for phosphorus acquisition. Plant Physiol 167:1430-1439.
777 https://doi.org/10.1104/pp.15.00145

778 Moir JO, Tiessen H Characterization of Available P by Sequential Extraction. 1-14.
779 https://doi.org/10.1201/9781420005271.ch25

780 Postma JA, Dathe A, Lynch JP (2014) The optimal lateral root branching density for maize depends
781 on nitrogen and phosphorus availability. Plant Physiol 166:590-602.
782 https://doi.org/10.1104/pp.113.233916

783 Postma JA, Lynch JP (2011) Root cortical aerenchyma enhances the growth of maize on soils with
784 suboptimal availability of nitrogen, phosphorus, and potassium. Plant Physiol 156:1190-

1201. https://doi.org/10.1104/pp.111.175489

Schneider HM, Klein SP, Hanlon MT, et al (2020) Genetic control of root architectural plasticity in maize. J Exp Bot 71:3185-3197. https://doi.org/10.1093/jxb/eraa084

Shen J, Yuan L, Zhang J, et al (2011) Phosphorus dynamics: from soil to plant. Plant Physiol 156:997-1005. https://doi.org/10.1104/pp.111.175232

Sun J, Zhao X, Fang Y, et al (2022) Root growth and architecture of tamarix chinensis in response to the groundwater level in the Yellow River delta. Mar Pollut Bull 179:113717. https://doi.org/10.1016/j.marpolbul.2022.113717

Tang Q, Wang G, Zhao L, et al (2023) Response of yield, root traits and plasticity of nitrogen-efficient cultivars of drip-irrigated rice to a nitrogen environment. J Integr Agric S2095311923004616. https://doi.org/10.1016/j.jia.2023.12.014

Vandamme E, Ahouanton K, Mwakasege L, et al (2018) Phosphorus micro-dosing as an entry point to sustainable intensification of rice systems in sub-Saharan Africa. Field Crops Res 222:39-49. https://doi.org/10.1016/j.fcr.2018.02.016

Wang G, Laga H, Jia J, et al (2020a) Statistical analysis and modeling of the geometry and topology of plant roots. J Theor Biol 486:110108. https://doi.org/10.1016/j.jtbi.2019.110108

Wang H, Siopongco J, Wade LJ, Yamauchi A (2009) Fractal analysis on root systems of rice plants in response to drought stress. Environ Exp Bot 65:338-344. https://doi.org/10.1016/j.envexpbot.2008.10.002

Wang X, Yan J, Zhang X, et al (2020b) Organic manure input improves soil water and nutrients use for sustainable maize (zea mays. L) productivity on the loess plateau. PLOS One 15:e0238042. https://doi.org/10.1371/journal.pone.0238042

Wang Y, Guo Z, Zhang S, et al (2025) Foliar application of γ-polyglutamic acid enhances growth, yield, and rhizosphere microbiota of summer maize under varied water regimes. Agronomy 15:754-767. https://doi.org/10.3390/agronomy15030754

Withers PJA (2019) Closing the phosphorus cycle. Nat Sustain 2:1001-1002. https://doi.org/10.1038/s41893-019-0428-6

Yang J, Zhou Q, Zhang J (2017) Moderate wetting and drying increases rice yield and reduces water use, grain arsenic level, and methane emission. Crop J 5:151-158. https://doi.org/10.1016/j.cj.2016.06.002

Yang L, Yang Z, Zhong X, et al (2021a) Decreases in soil P availability are associated with soil organic P declines following forest conversion in subtropical china. Catena 205:105459. https://doi.org/10.1016/j.catena.2021.105459

Yang L, Yang Z, Zhong X, et al (2021b) Decreases in soil P availability are associated with soil

organic P declines following forest conversion in subtropical china. Catena 205:105459. https://doi.org/10.1016/j.catena.2021.105459

Yang T, Zhao J, Hong M, et al (2025) Optimizing water and nitrogen supply can regulate the dynamics of dry matter accumulation in maize, thereby promoting dry matter accumulation and increasing yield. Field Crops Res 326:109837. https://doi.org/10.1016/j.fcr.2025.109837

York LM, Carminati A, Mooney SJ, et al (2016) The holistic rhizosphere: integrating zones, processes, and semantics in the soil influenced by roots. J Exp Bot 67:3629-3643. https://doi.org/10.1093/jxb/erw108

Zeng W, Hou Y, Ao C, Huang J (2024) Effects of PGPR and γ-PGA on maize growth and rhizosphere microbial community in saline soil. Agric Water Manag 295:108736. https://doi.org/10.1016/j.agwat.2024.108736

Zhou T, Li X, Zhang Y, et al (2026) Water-saving irrigation enhances rice P uptake by raising soil labile P and improving root traits. Field Crops Res 341:110419. https://doi.org/10.1016/j.fcr.2026.110419

Zhou Y, Li Z, Li Y, et al (2025) Moderate deep banding of phosphorus enhanced winter wheat yield and fertilizer uptake efficiency by promoting nutrient absorption and translocation of pre-anthesis nutrient. Field Crops Res 322:109728. https://doi.org/10.1016/j.fcr.2024.109728

Zhu Y, Zhang L, Zhang W, et al (2026) γ-polyglutamic acid alleviates chromium toxicity in tobacco plants: physiological regulation and microbial mechanism. Ecotoxicol Environ Saf 310:119756. https://doi.org/10.1016/j.ecoenv.2026.119756